



POLITECNICO DI TORINO

Master Degree course in Data Science and Engineering

Mathematical Models for Biomedicine

Study of ‘Agent-Based and Continuum Models for Spatial Dynamics of Infection by Oncolytic Viruses’

Professors

Prof. Chiara GIVERSO
Prof. Luigi PREZIOSI
Prof. Luca MESIN

Student

Gustavo NICOLETTI ROSA

ACADEMIC YEAR 2023-2024

Contents

1	Introduction	3
1.1	Experimental observations	3
1.2	Models in literature	4
1.2.1	Dunbar	4
1.2.2	Pooladvand	5
1.2.3	Malinzi	5
1.2.4	Dongwook	5
1.2.5	Guo	5
2	Methods	7
2.1	Deduction of the model	7
2.1.1	Deriving continuum model	7
2.2	Qualitative analysis	11
2.2.1	Equilibria	11
2.2.2	Travelling waves	14
3	Results	15
3.1	Numerical simulations	15
3.1.1	1D Undirected	15
3.1.2	2D Undirected	16
3.1.3	1D Pressure-Driven	18
3.1.4	2D Pressure-Driven	18
3.1.5	Other parameters	20
3.2	Conclusion	22
	Bibliography	23

Chapter 1

Introduction

Oncolytic viruses (OVs) have gained increasing attention in cancer research thanks to genetic engineering, giving rise to genetically modified oncolytic viruses (GMOVs). The virus preferably infects tumor cells thanks to the increase of some receptors (e.g. CD54) on the external membrane of tumor cells and lower immunity against viruses, causing oncolysis, and research has found that there might be beneficial synergies with immunotherapy, especially because OVs may cause immunogenic cell death and because the oncolysis releases tumor-associated antigens (TAA), neoantigens (TAN) and damage-associated molecular patterns (DAMPs), increasing the efficacy of the immunologic system, GMOVs can even enhance the representation of the antigens [6]. However the spatial dynamics of the infection are still not well understood, this report will discuss the model proposed by Morselli et al. (2023) [9], based on a stochastic agent-based model describing infected and uninfected solid tumors; we considered two types of movements: undirected random and pressure-driven, and derived the continuum limit. The study is carried out in one and two dimensions.

The treatment is done by administering the OVs through intra-tumoral injection, the viruses will selectively infect tumor cells locking them in the S-phase, making it so the infected tumor cell will not replicate, and our model considers simply a death rate of the infected cells, without considering the interaction with the immunologic system.

1.1 Experimental observations

A study by Berg et al. (2019) [2] performed *in vitro* experiments of the oncolytic measles virus MVeGFP infecting HT1080 fibrosarcoma cells in 2D and 3D, the paper confirms that viruses predominantly infect from cell to cell in their neighborhood, validating our future assumptions for this paper's model, in addition, they also observed that some tumor cells remained uninfected for the duration of the study despite being near highly infectious foci.

From the need to better understand the spatial characteristics of the OV infection, in an article by Wodarz et al. (2012) [12] in another *in vitro* experiment, with embryonic kidney 293 cells (K293) spread in 2D and a recombinant adenovirus type-5 (Ad5) that expresses enhanced jellyfish green fluorescent protein (EGFP), therefore not tumor cells

and OV, but the results are interesting for the spatial interaction. They observed three patterns: *hollow ring* (i), i.e. the infected cells growing in a ring structure, leaving only dead cells in the middle; *disperse* (ii), in which the infection is separated in mixed clusters; and *filled ring* (iii) again having a high density of infected cells in a ring, but the center is still filled with uninfected cells, observable in Fig. 1.1, Morselli's model with the reference parameters and unbiased movement will produce the third pattern and by changing the initial conditions, we produced the second pattern. An important matter is how to change the parameters to have an effective treatment with OVs.

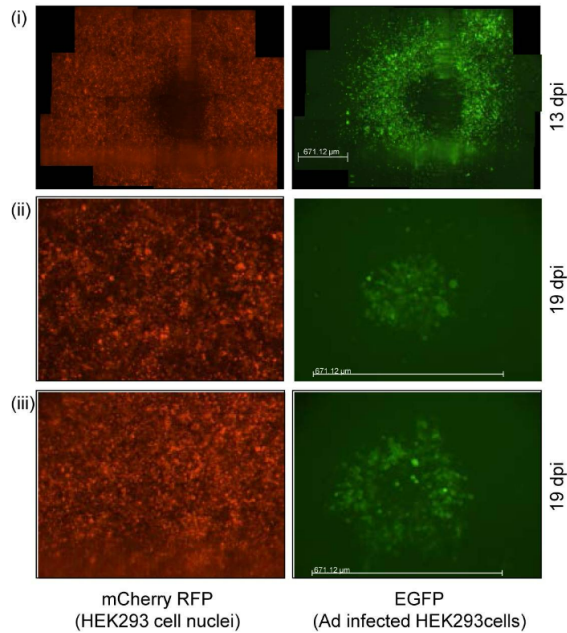


Figure 1.1: Portion of the original image from Wodarz et al. (2012) [12], on the left uninfected K293 cells, on the right infected K293 cells by Ad5, each row show a pattern of infection, and the times 13 or 19 days post-inoculation (dpi).

1.2 Models in literature

1.2.1 Dunbar

Dunbar (1984) [4] proposed a similar continuum prey-predator model for which he proved the existence of a traveling wave solution for the model (1.1). The difference between Morselli's continuum model (2.8) and Dunbar's is that the latter does not consider w (Morselli's i) to contribute to reaching the carrying capacity.

$$\begin{cases} \partial_t u &= D_1 \partial_{xx}^2 u + Au(1 - \frac{u}{K}) - Buw \\ \partial_t w &= D_2 \partial_{xx}^2 w - Cw + Euw \end{cases} \quad (1.1)$$

1.2.2 Pooladvand

Pooladvand et al. (2021) [10] proposes a continuum model with spherical symmetry (1.2) for oncolytic virotherapy but with more terms concerning the free virus dynamics, such as the increase of virions given the burst of an infected cell δ_I , scaled by α ; and the rate of infection β for which free viruses can enter both U and I , so their model is more complicated. Their paper contains an analysis of a range of values of parameters creating different bifurcation diagrams.

$$\begin{cases} \frac{\partial U}{\partial t} = \frac{D_u}{r^2} \frac{\partial}{\partial r} \left(r^2 \frac{\partial U}{\partial r} \right) + r_U U \left(1 - \frac{U+I}{k} \right) - \beta UV \\ \frac{\partial V}{\partial t} = \frac{D_v}{r^2} \frac{\partial}{\partial r} \left(r^2 \frac{\partial V}{\partial r} \right) - \delta_v V - \beta(U+I)V + \alpha\delta_I I \\ \frac{\partial I}{\partial t} = \frac{D_u}{r^2} \frac{\partial}{\partial r} \left(r^2 \frac{\partial I}{\partial r} \right) + \beta UV - \delta_I I \end{cases} \quad (1.2)$$

1.2.3 Malinzi

Malinzi et al. (2017) [7] models chemovirotherapy (1.3), where U, I, V, C are, respectively, uninfected tumor cells, infected tumor cells, free viruses, and drug concentration. I and U have additional interaction terms with the drug, and the latter can be administered in time following the function $C_b(t)$.

$$\begin{cases} \frac{\partial U}{\partial t} = D_1 \frac{1}{r^2} \frac{\partial}{\partial r} \left[r^2 \frac{\partial U}{\partial r} \right] + \alpha U \left(1 - \frac{U+I}{K} \right) - \frac{\beta UV}{K_u+U} - \frac{\delta_0 UC}{K_c+C} \\ \frac{\partial I}{\partial t} = D_2 \frac{1}{r^2} \frac{\partial}{\partial r} \left[r^2 \frac{\partial I}{\partial r} \right] + \frac{\beta UV}{(K_u+U)} - \frac{\delta_I IC}{K_c+C} - \delta_I I \\ \frac{\partial V}{\partial t} = D_3 \frac{1}{r^2} \frac{\partial}{\partial r} \left[r^2 \frac{\partial V}{\partial r} \right] + b\delta I - \frac{\beta UV}{K_u+U} - \gamma V \\ \frac{\partial C}{\partial t} = D_4 \frac{1}{r^2} \frac{\partial}{\partial r} \left[r^2 \frac{\partial C}{\partial r} \right] + C_b(t) - \mu C \end{cases} \quad (1.3)$$

1.2.4 Dongwook

Dongwook et al. (2022) [8] models (1.4) cancer cells x , infected cells y , free virions v , and natural killer (NK) cells z which is a virus-induced immune response, indeed, in the model the growth factor of z depends on the presence of y and z can kill both x and y with different rates. The model lacks spatial dynamics.

$$\begin{cases} \frac{\partial x}{\partial t} = \lambda x \left(1 - \frac{x}{K} \right) - \alpha xv - \beta xz \\ \frac{\partial y}{\partial t} = \alpha xv - \gamma yz - \delta_1 y \\ \frac{\partial v}{\partial t} = b\delta_1 y - \alpha xv - \delta_2 v \\ \frac{\partial z}{\partial t} = \lambda_z yz - \delta_3 z \end{cases} \quad (1.4)$$

1.2.5 Guo

Guo et al. (2023) [5] models (1.5) tumor cells T , infected cells I , infected cells in the eclipse phase E , free virions V , and the interferon response F , a protein produced by the immunologic system in response to the presence of the infection. Differently from the

previous model, these proteins cannot kill cells nor free viruses, rather, they reduce the production of V in the domain, and the model does not consider the release of V in the event of lysis of I , but considers only their release while the infected cell is still alive and not in the eclipse phase. The model lacks spatial dynamics.

$$\begin{cases} \frac{\partial T}{\partial t} &= \lambda T - \beta TV \\ \frac{\partial E}{\partial t} &= \beta TV - kE \\ \frac{\partial I}{\partial t} &= kE - \delta I \\ \frac{\partial V}{\partial t} &= I \left(\frac{p}{1+\epsilon F} \right) - cV \\ \frac{\partial F}{\partial t} &= V - \alpha F \end{cases} \quad (1.5)$$

Chapter 2

Methods

2.1 Deduction of the model

Morselli's model proposes a stochastic agent-based model defining the temporal discretization $t_n = \tau n$ and spatial discretization $x_j = \delta j$, cells occupying position x_j in time t_n are uninfected U_j^n and infected tumor cells I_j^n , the densities are $u_j^n = U_j^n/\delta$ and $i_j^n = I_j^n/\delta$. We define $\rho_j^n = u_j^n + i_j^n$ the barotropic relation. The cells will have the following action probabilities:

Uninfected		Infected	
Proliferation	$\tau G(\rho_j^n)_+$	Die	τq
Die	$\tau G(\rho_j^n)_-$	Move	$\tilde{F}_{j \rightarrow j \pm 1}^n$
Be infected	$\tau \frac{\beta}{K} i_j^n$		
Move	$F_{j \rightarrow j \pm 1}^n$		

Table 2.1: Set of action and probabilities for cells

Uninfected has growth function $G(\rho) = p(1 - \frac{\rho}{P})$, we notice that the probability of reproducing reduces as the pressure increases till reaching the homeostatic pressure P and it dies only when above such pressure which corresponds to the carrying capacity of the system $K > 0$. As for the movement of cells, we used $F_{j \rightarrow j \pm 1}^n = \tilde{F}_{j \rightarrow j \pm 1}^n = \theta/2$ in case of standard unbiased random walk or $F_{j \rightarrow j \pm 1}^n = \tilde{F}_{j \rightarrow j \pm 1}^n = \theta \frac{(\rho_j^n - \rho_{j \pm 1}^n)_+}{2P}$ for pressure-driven random movement, with $\theta = \theta_u = \theta_i$ the mobility coefficients. The proliferation of infected cells is not modeled for the virus disrupts this ability in the cell, and it dies with a constant death rate $q > 0$. The probability of infecting uninfected depends on the number of infected cells inside the discrete position x_j , and is proportional to the infection rate $\beta > 0$ normalized by the carrying capacity K .

2.1.1 Deriving continuum model

We have that the concentration of uninfected cells at time t_{n+1} in position x_j is given by the probability of uninfected cells moving in, moving out, or staying, times the rate of

reproducing or dying explicated by the multiplication factor $[1 + \tau G(\rho)]$ times the rate of not being infected:

$$u_j^{n+1} = [F_{j-1 \rightarrow j}^n u_{j-1}^n + F_{j+1 \rightarrow j}^n u_{j+1}^n + (1 - F_{j \rightarrow j-1}^n - F_{j \rightarrow j+1}^n) u_j^n] [1 + \tau G(\rho_j^n)] (1 - \tau \frac{\beta}{K} i_j^n) \quad (2.1)$$

We define

$$\Phi := -(F_{j \rightarrow j-1}^n + F_{j \rightarrow j+1}^n) u_j^n + F_{j-1 \rightarrow j}^n u_{j-1}^n + F_{j+1 \rightarrow j}^n u_{j+1}^n \quad (2.2)$$

Hence (2.1) becomes:

$$\begin{aligned} u_j^{n+1} &= (u_j^n + \Phi) [1 + \tau G(\rho_j^n)] (1 - \tau \frac{\beta}{K} i_j^n) \\ &= u_j^n + \tau G(\rho_j^n) u_j^n - \tau \frac{\beta}{K} u_j^n i_j^n + \Phi - \tau^2 G(\rho_j^n) \frac{\beta}{K} u_j^n i_j^n \\ &\quad + \tau \Phi [G(\rho_j^n) - \frac{\beta}{K} i_j^n - \tau G(\rho_j^n) \frac{\beta}{K} i_j^n] \end{aligned}$$

We can rearrange:

$$\frac{u_j^{n+1} - u_j^n}{\tau} = G(\rho_j^n) u_j^n - \frac{\beta}{K} u_j^n i_j^n + \frac{\Phi}{\tau} + H_1 \quad (2.3)$$

where

$$H_1 := -\tau G(\rho_j^n) \frac{\beta}{K} u_j^n i_j^n + \Phi [G(\rho_j^n) - \frac{\beta}{K} i_j^n - \tau G(\rho_j^n) \frac{\beta}{K} i_j^n]$$

H_1 contains higher order terms of the soon-vanishing variables $\tau, \delta \rightarrow 0$. We can assume the necessary regularity conditions to compute the Taylor expansions for u both in time and space and for ρ in space.

$$\begin{aligned} u_j^{n+1} &= u(t_n + \tau, x_j) = u + \tau \partial_t u + O(\tau^2) \\ u_{j \pm 1}^n &= u(t_n, x_j \pm \delta) = u \pm \delta \partial_x u + \frac{1}{2} \delta^2 \partial_{xx}^2 u + O(\delta^3) \\ \rho_{j \pm 1}^n &= \rho(t_n, x_j \pm \delta) = \rho \pm \delta \partial_x \rho + \frac{1}{2} \delta^2 \partial_{xx}^2 \rho + O(\delta^3) \end{aligned}$$

Unbiased Random Walk

In the unbiased random movement, we have $F_{j \rightarrow j \pm 1}^n = F_{j \pm 1 \rightarrow j}^n = \theta_u/2$ constant. We obtain

$$\Phi = \frac{\theta_u}{2} (u_{j-1}^n + u_{j+1}^n - 2u_j^n) = \frac{\theta_u}{2} \delta^2 \partial_{xx}^2 u + O(\delta^3)$$

And

$$H_1 = O(\tau) + O(\delta^2)$$

Hence (2.3) becomes

$$\partial_t u + O(\tau^2) = \theta_u \frac{\delta^2}{2\tau} \partial_{xx}^2 u + G(\rho) u - \frac{\beta}{K} u i + O(\tau) + O(\delta^2) \quad (2.4)$$

With $\tau, \delta \rightarrow 0$ such that $\frac{\delta^2}{2\tau} \rightarrow D$:

$$\partial_t u = \theta_u D \partial_{xx}^2 u + G(\rho)u - \frac{\beta}{K} ui \quad (2.5)$$

Infected cells concentration i_j^{n+1} depends on the probability of infected cells moving in or staying, times the rate of not dying, plus the infection of uninfected cells that may move, stay, reproduce, or die, giving rise to the following:

$$i_j^{n+1} = [\tilde{F}_{j-1 \rightarrow j}^n i_{j-1}^n + \tilde{F}_{j+1 \rightarrow j}^n i_{j+1}^n + (1 - \tilde{F}_{j \rightarrow j-1}^n - \tilde{F}_{j \rightarrow j+1}^n) i_j^n] (1 - \tau q) \\ + \tau \frac{\beta}{K} i_j^n [1 + \tau G(\rho_j^n)] [F_{j-1 \rightarrow j}^n u_{j-1}^n + F_{j+1 \rightarrow j}^n u_{j+1}^n + (1 - F_{j \rightarrow j-1}^n - F_{j \rightarrow j+1}^n) u_j^n]$$

With the same type of procedure as before, we obtain:

$$\partial_t i = \theta_i D \partial_{xx}^2 i + \frac{\beta}{K} ui - qi \quad (2.6)$$

Pressure-Driven Cell Movement

For uninfected cells, we have with the Taylor expansion of ρ :

$$F_{j \rightarrow j \pm 1}^n := \theta_u \frac{(\rho_j^n - \rho_{j \pm 1}^n)_+}{2P} = \frac{\theta_u}{2P} (\pm \delta \partial_x \rho + \frac{1}{2} \delta^2 \partial_{xx}^2 \rho + O(\delta^3))_+$$

Now using the Taylor expansion of u :

$$\begin{aligned} \Phi &= -(F_{j \rightarrow j-1}^n + F_{j \rightarrow j+1}^n)u + F_{j-1 \rightarrow j}^n(u - \delta \partial_x u + \frac{1}{2} \delta^2 \partial_{xx}^2 u + O(\delta^3)) \\ &\quad + F_{j+1 \rightarrow j}^n(u + \delta \partial_x u + \frac{1}{2} \delta^2 \partial_{xx}^2 u + O(\delta^3)) \\ &= (F_{j-1 \rightarrow j}^n - F_{j \rightarrow j-1}^n + F_{j+1 \rightarrow j}^n - F_{j \rightarrow j+1}^n)u + \delta(-F_{j-1 \rightarrow j}^n + F_{j+1 \rightarrow j}^n) \partial_x u \\ &\quad + \frac{1}{2} \delta^2 (F_{j-1 \rightarrow j}^n + F_{j+1 \rightarrow j}^n) \partial_{xx}^2 u + O(\delta^3) \end{aligned}$$

We observe that

$$\begin{aligned} F_{j \pm 1 \rightarrow j}^n - F_{j \rightarrow j \pm 1}^n &= \frac{\theta_u}{2P} [(\rho_{j \pm 1}^n - \rho_j^n)_+ - (\rho_j^n - \rho_{j \pm 1}^n)_+] \\ &= \frac{\theta_u}{2P} (\rho_{j \pm 1}^n - \rho_j^n) \\ &= \frac{\theta_u}{2P} (\pm \delta \partial_x \rho + \frac{1}{2} \delta^2 \partial_{xx}^2 \rho + O(\delta^3)) \end{aligned}$$

We have

$$\Phi = \frac{\theta_u}{2P} \{ \delta^2 \partial_{xx}^2 \rho u + \delta[-(-\delta \partial_x \rho + O(\delta^2))_+ + (\delta \partial_x \rho + O(\delta^2))_+] \partial_x u + O(\delta^3) \}$$

Hence (2.3) becomes

$$\begin{aligned} \partial_t u + O(\tau^2) &= G(\rho)u - \frac{\beta}{K} ui \\ &\quad + \frac{\theta_u}{P} \frac{\delta^2}{2\tau} \{ \partial_{xx}^2 \rho u + [(\partial_x \rho + O(\delta))_+ - (-\partial_x \rho + O(\delta))_+] \partial_x u + O(\delta) \} + H_1 \end{aligned}$$

Finally, with $\tau, \delta \rightarrow 0$ such that $\frac{\delta^2}{2\tau} \rightarrow D$:

$$\begin{aligned}\partial_t u &= \frac{\theta_u D}{P} \{ \partial_{xx}^2 \rho u + [(\partial_x \rho)_+ - (-\partial_x \rho)_+] \partial_x u \} + G(\rho) u - \frac{\beta}{K} ui \\ &= \frac{\theta_u D}{P} (\partial_{xx}^2 \rho u + \partial_x \rho \partial_x u) + G(\rho) u - \frac{\beta}{K} ui \\ &= \frac{\theta_u D}{P} \partial_x (u \partial_x \rho) + G(\rho) u - \frac{\beta}{K} ui\end{aligned}$$

Similarly for infected cells

$$\partial_t i = \frac{\theta_i D}{P} \partial_x (i \partial_x \rho) + \frac{\beta}{K} ui - qi \quad (2.7)$$

Hence, with $D_u = \theta_u D$ and $D_i = \theta_i D$ for Random movement, and $G(\rho) = p(1 - \frac{\rho}{P})$ logistic growth, $P = K$ and $\rho = u + i$, the continuum model is

$$\begin{cases} \partial_t u = D_u \partial_{xx}^2 u + up(1 - \frac{u+i}{K}) - \frac{\beta}{K} ui \\ \partial_t i = D_i \partial_{xx}^2 i + \frac{\beta}{K} ui - qi \end{cases} \quad (2.8)$$

And for Pressure-Driven movement

$$\begin{cases} \partial_t u = \frac{D_u}{P} \partial_x (u \partial_x \rho) + up(1 - \frac{u+i}{K}) - \frac{\beta}{K} ui \\ \partial_t i = \frac{D_i}{P} \partial_x (i \partial_x \rho) + \frac{\beta}{K} ui - qi \end{cases} \quad (2.9)$$

2.2 Qualitative analysis

We use well-known results from traveling waves for the random movement (2.8), but analytical results are still unavailable for the pressure-driven model. The spatially homogeneous system of our model for both types of movements is

$$\begin{cases} \partial_t u = up(1 - \frac{u+i}{K}) - \frac{\beta}{K}ui \\ \partial_t i = \frac{\beta}{K}ui - qi \end{cases} \quad (2.10)$$

2.2.1 Equilibria

From this system of equations, we get three equilibria: $(0,0)$, both populations missing; $(K,0)$, only uninfected cells; and (u^*, i^*) such that

$$(u^*, i^*) = \left(\frac{qK}{\beta}, \frac{pK(\beta - q)}{\beta(\beta + p)} \right) \quad (2.11)$$

By computing the eigenvalues of the Jacobian matrix in such points we evaluate the stability:

$$J(u, i) = \begin{pmatrix} p \left(1 - \frac{2u+i}{K}\right) - \frac{\beta}{K}i & \frac{u}{K}(p - \beta) \\ \frac{\beta i}{K} & \frac{\beta u}{K} - q \end{pmatrix} \quad (2.12)$$

We get that the eigenvalues of $(0,0)$ are $\{p, -q\}$, so it is unstable, for $(K,0)$ are $\{-p, \beta - q\}$, which is stable only for $\beta < q$, and (u^*, i^*) have eigenvalues whose sum is $-\frac{pq}{\beta}$ and product is $\frac{pq(\beta - q)}{\beta}$, for i^* to be positive, we need $\beta > q$, hence the product of the eigenvalues is positive, and the sum is negative, therefore both eigenvalues have negative real part, giving rise to a stable equilibrium. If we consider $\beta < q$ the only stable equilibrium is the extinction of infected cells, and failure of the treatment, so we are interested in the case $\beta > q$, and the traveling wave connecting $(0,0)$ to (u^*, i^*) since we are treating a tumor that still has to grow. With the parameters used in the paper by Morselli, described in Tab. 3.1, we have $(u^*, i^*) \approx (409, 92)$ in 1D and $(u^*, i^*) \approx (4088, 916)$ in 2D, which will be the expected value of the concentrations in the region where the waves have already passed by, as we will notice in the next section.

By setting the maps $\tilde{u}(i) : \partial_t u = 0$

$$\tilde{u}(i) = \frac{qK}{\beta}$$

and $\tilde{i}(u) : \partial_t i = 0$, with the linear relation

$$\tilde{i}(u) = u \left(\frac{-p}{p + \beta} \right) + \frac{pK}{p + \beta}$$

We can plot the phase graph with the equilibrium points as in Fig. 2.1. We observe that both unstable equilibria are saddle points, and the stable equilibrium is a node.

Now we plot the corresponding bifurcation diagrams for the parameters β, q, p against the equilibrium points of u and i .

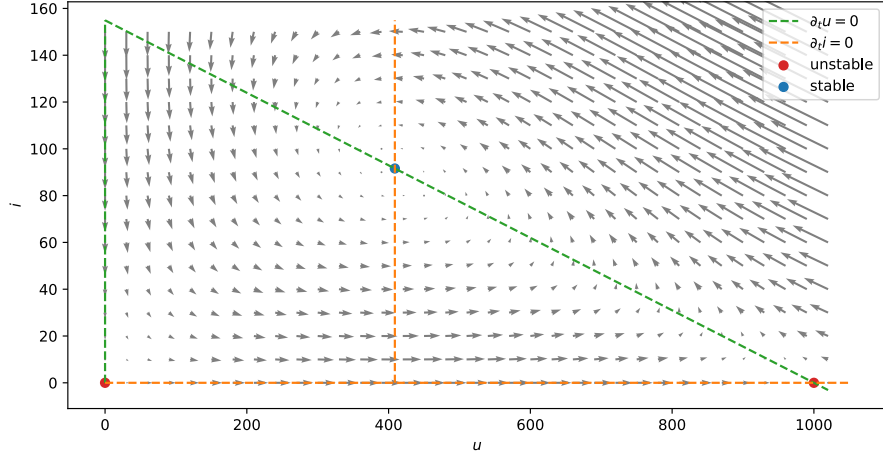
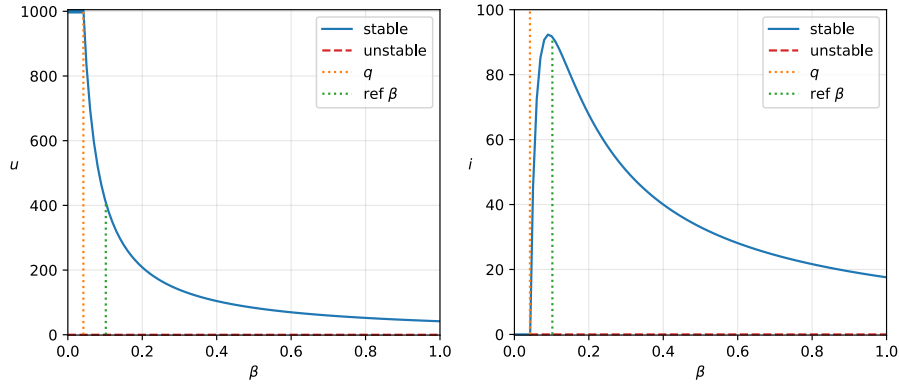


Figure 2.1: Phase graph of spatially homogeneous analog model

Bifurcation for β


 Figure 2.2: Bifurcation diagram for $(u, i) \times \beta$

In Fig. 2.2, we notice that the only stable equilibrium for $\beta < q$ is $(K, 0)$, because the infected cells end up dying faster than they infect, and $u(\beta) = 0$ is unstable because a single tumor cell would eventually replicate until the carrying capacity K . Whereas for $\beta > q$, the stable equilibrium is given by the expression for (u^*, i^*) in (2.11), $u(\beta)$ is hyperbolic and $i(\beta)$ for $\beta \rightarrow +\infty$, is also hyperbolic converging to 0, as u decreases to zero thanks to the high infection rate, and eventually the infected cells will die, hence such convergence; in this interval $i(\beta) = 0$ is unstable because a small disturbance would start an infection that would stabilize at the values (u^*, i^*) . The maximum value of i ,

$\max i(\beta)$, is given by finding $\bar{\beta} : \partial_\beta i = 0$ as in the following equation, with $\beta > q > 0$:

$$\frac{\partial}{\partial \beta} \left(\frac{pK(\beta - q)}{\beta(\beta + p)} \right) = 0 \implies \bar{\beta} = q + \sqrt{q^2 + pq}$$

Bifurcation for q

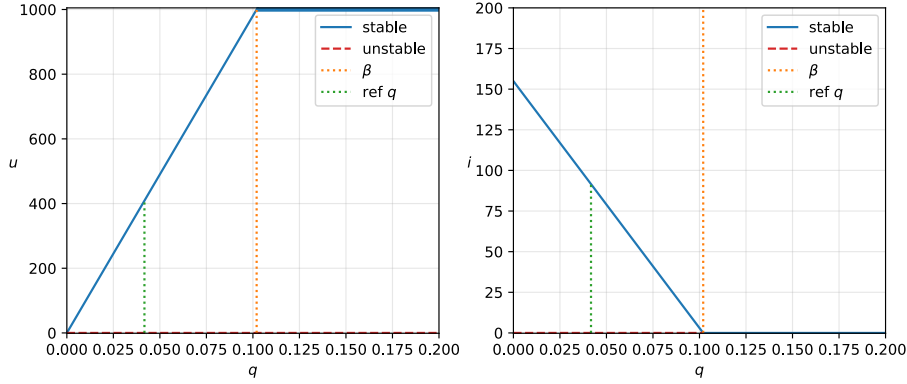


Figure 2.3: Bifurcation diagram for $(u, i) \times q$

In Fig. 2.3 we notice the same condition for $q < \beta$, the infected cells die slower than they can infect, but this time we notice a linear dependency for the equilibrium (u^*, i^*) , the maximum value of $i(q)$ is different in this graph because when $q = 0$, the q line in Fig. 2.2 tends to zero, the orange vertical line shifts, increasing the maximum value of the dynamics when varying β . When $q > \beta$ the stable equilibrium is again $(K, 0)$.

Bifurcation for p

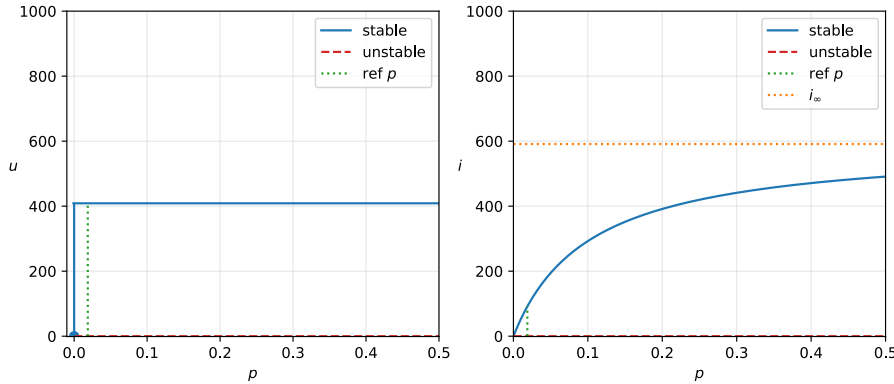


Figure 2.4: Bifurcation diagram for $(u, i) \times p$

In Fig. 2.4 we observe that $u(p) = u^*$ constant, for $p > 0$. Observing $i(p)$ we notice that even though the uninfected cells' growing factor p does not change the equilibrium point u^* , it does change the number of infected cells in the stable equilibrium, there is a hyperbolic convergence towards $i_\infty = \lim_{p \rightarrow +\infty} i^*(p) = K - u^*$, reaching the state where the sum of u and i equals the carrying capacity.

2.2.2 Travelling waves

In the unbiased movement setting, to study the minimum velocity of the traveling wave of infected cells we consider the case that the concentration of uninfected cells is constant \hat{u} in the invading region:

$$\partial_t i = D_i \partial_{xx}^2 + \left(\frac{\beta}{K} \hat{u} - q \right) i$$

Van Saarloos (2003) [11] proved that an equation of the form $\partial_t y = D \partial_{xx}^2 y + f(y)$ with compact initial conditions yields a traveling wave solution with minimum speed $c = 2\sqrt{D\alpha}$ such that $f'(0) = \alpha$. So we expect the uninfected wavefront travel at minimum speed $c_u = 2\sqrt{D_u p}$ whilst the infected at minimum speed $c_i = 2\sqrt{D_i(\frac{\beta}{K}\hat{u} - q)}$, and for $\hat{u} = K$ we get $c_i = 2\sqrt{D_i(\beta - q)}$. However, the infection reduces the peak density of the wavefront of the uninfected cells, reducing the speed of propagation of the infected wavefront c_i .

We can calculate the expected peak of the uninfected wavefront by solving for \bar{u} the equation for when both wavefronts reach the same velocity, keeping a constant distance at convergence:

$$c_u = 2\sqrt{D_u p} = 2\sqrt{D_i \left(\frac{\beta}{K} \bar{u} - q \right)} = c_i \quad (2.13)$$

Solving, we get

$$\bar{u} = \left(\frac{q}{\beta} + \frac{D_u p}{D_i \beta} \right) K = u^* + \frac{D_u p K}{D_i \beta} \quad (2.14)$$

In the pressure-driven movement, by Aronson (1980) [1] and other density-dependent interaction-diffusion, we obtain that the solution is sharp waves with minimum velocity $c_u = \sqrt{D_u p / 2}$.

Chapter 3

Results

3.1 Numerical simulations

The parameters we used are listed in Tab. 3.1, based on the ones used in the original paper, in addition, we ran our agent-based-model (ABM) simulations with spatial discretization $\delta = 0.05\text{mm}$ and temporal discretization $\tau = 0.2\text{h}$, from which we took the average in space for each specific hour, and simulated the continuum model with py-pde library [13] and with the Upwind method [3] to deal with the numerical instabilities that will be briefly discussed.

Parameter	Description	Value (Units)
p	Maximal duplication rate of uninfected cells	$1.87 \times 10^{-2}(\text{h}^{-1})$
q	Death rate of infected cells	$4.17 \times 10^{-2}(\text{h}^{-1})$
D_u, D_i	Diffusion coefficients (undirected)	$1.88 \times 10^{-4}(\text{mm}^2/\text{h})$
D_u, D_i	Diffusion coefficients (pressure-driven)	$1.50 \times 10^{-3}(\text{mm}^2/\text{h})$
$K^{1\text{D}}$	Tissue carrying capacity in one dimension	$10^3(\text{cells/mm})$
$K^{2\text{D}}$	Tissue carrying capacity in two dimension	$10^4(\text{cells/mm}^2)$
β	Infection rate	$1.02 \times 10^{-1}(\text{h}^{-1})$
R_u	Initial radius of uninfected cells	$2.6(\text{mm})$
R_i	Initial radius of infected cells	$1.0(\text{mm})$

Table 3.1: Reference parameters

Our initial conditions are given by

$$u_0(x) = \begin{cases} 0.9K & \text{for } |x| \leq R_u \\ 0 & \text{for } |x| > R_u \end{cases} \quad i_0(x) = \begin{cases} 0.1K & \text{for } |x| \leq R_i \\ 0 & \text{for } |x| > R_i \end{cases} \quad (3.1)$$

3.1.1 1D Undirected

We start our simulations by plotting in Fig 3.1 the expected trajectory of the spatially homogeneous dynamic system (2.10) with initial conditions also used in future numerical

simulations, that is $(u_0, i_0) = (0.9K, 0.1K) = (900, 100)$ for the 1D case, and we observe the oscillations around the stable equilibrium. Still, it should strictly converge at $t \rightarrow +\infty$. So we can expect such oscillations and convergence also in our original model with spatial diffusion.

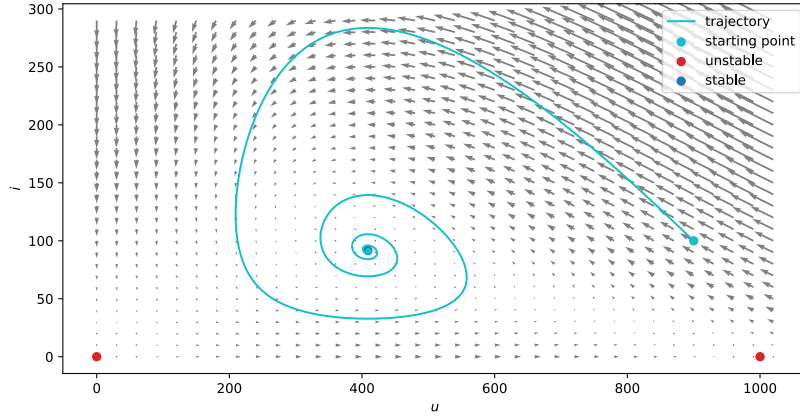


Figure 3.1: Trajectory in phase graph of spatially homogeneous analog, with starting conditions (u_0, i_0)

In Fig. 3.2 we plotted such results for the hours 80, 310, 700, 1000, averaging five ABM simulations and the solutions from the continuum model, together with results obtained in the qualitative analysis section (2.2): The blue and red solid lines are respectively the average over the simulations of u and i ; the dotted black line is the result of the continuum model; the horizontal grey line is the equilibrium point for the spatially homogeneous system in Eq.(2.10); the vertical dashed lines in cyan and red are, for u and i respectively, the expected front-wave position considering $R + ct$, for the latter however, as previously discussed, our approximation loses biological meaning as the velocity of infected wavefront reaches the velocity of the uninfected wavefront; finally the horizontal yellow solid line represents the expected uninfected wavefront density \bar{u} from Eq. (2.13).

3.1.2 2D Undirected

We ran three ABM simulations, with spatial discretization $\delta = 0.1\text{mm}$ and temporal discretization $\tau = 0.2\text{h}$, from which we took the average in space, and simulated the continuum model in Fig. 3.3, confirming the validity of the deduced continuum model also in two dimensions. Each 2D simulation took more than 30h to complete, to reduce the computational time, we used the concept of population unit `pop_unit` = 2 for u only, i.e. the action that would be taken by a single u cell is taken by `pop_unit` cells, such technique was not used for i because of the reduced number of cells, the approximation of the action distribution would not be as appropriate. In Fig. 3.4 we plotted average ABM results for the hours 80, 500, 1000.

Results

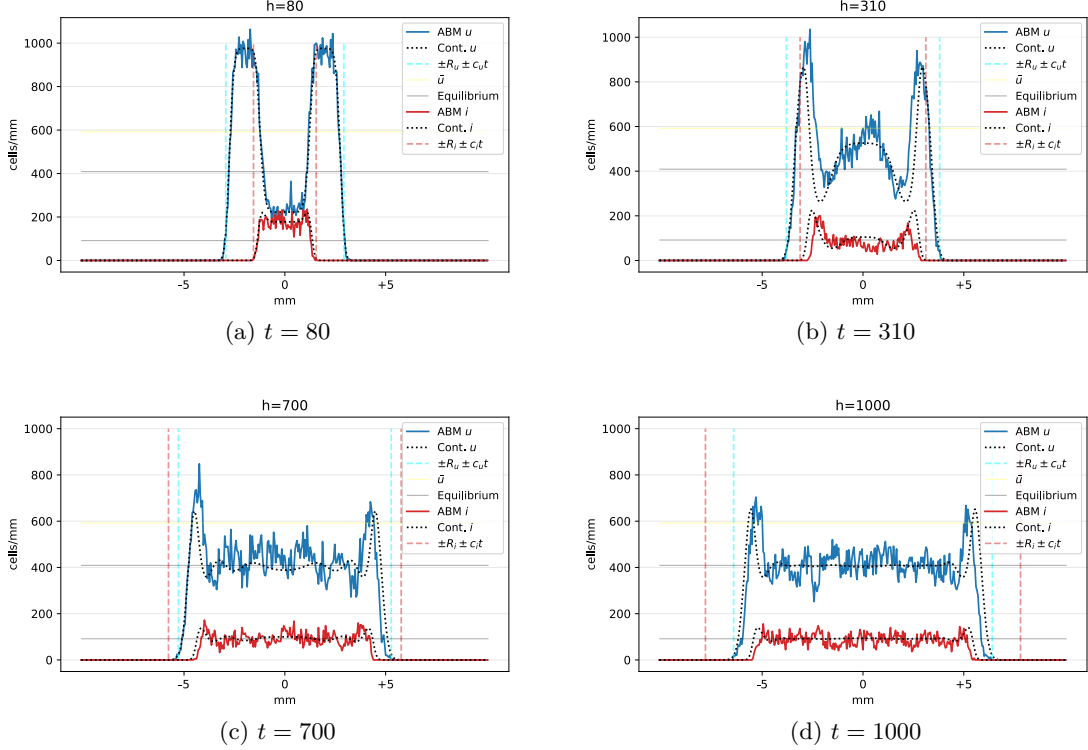


Figure 3.2: Results of 1D random movement simulations of ABM average and continuum model

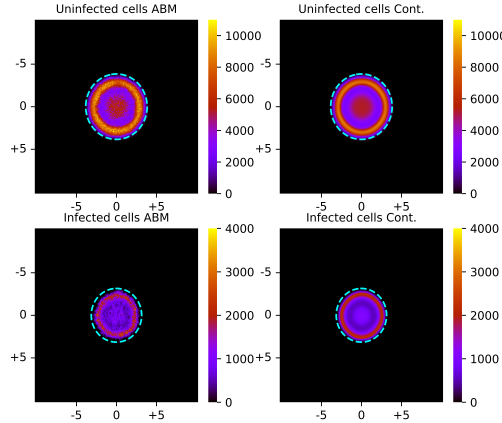


Figure 3.3: Results of 2D random movement simulations of ABM average and continuum model at time $t = 310$

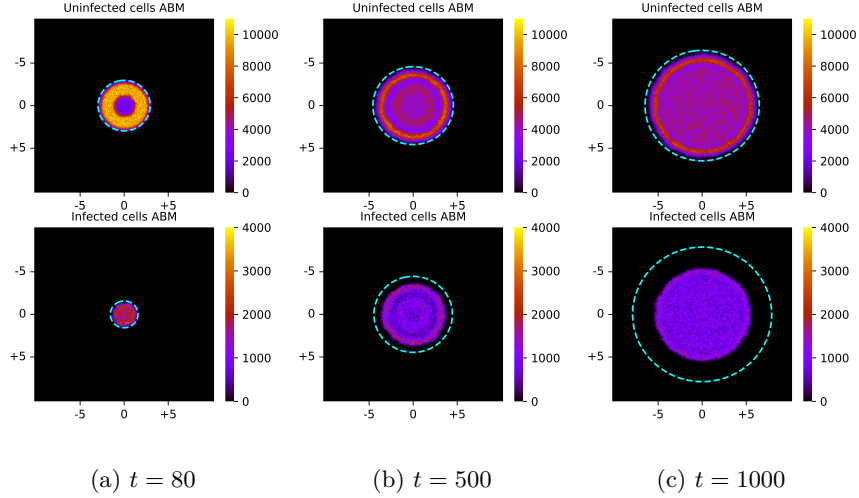


Figure 3.4: Results of 2D random movement simulations of ABM average

3.1.3 1D Pressure-Driven

In Fig. 3.5 we plotted the average of three ABM simulations and the continuum model solution for the hours 10, 70, 600, 1000. We notice a big difference with respect to the undirected movement model: the infection can barely propagate out of the initial radius because of the pressure gradient that is created by the infection and death of cells, these cannot leave the valley, whereas u cells outside it can 'fall in' it, the ABM simulations represent this effect very well. At greater time steps, i.e. $h = 1000$, the continuum solution and the ABM maintain the coherence of values for the diffusion front of u , with minimum propagation speed $c_u = \sqrt{D_u p/2}$. The continuum model converges to the expected equilibrium we calculated in section 2.2 where both waves of u and i have been through. We notice uninfected cells reaching carrying capacity outside the valley, and the infection does not spread, meaning a clear failure of the treatment.

To numerically solve the continuum model, the standard methods implemented by the library py-pde [13] introduced a high error due to the extreme pressure gradients in the valley of cells. Hence we used Upwind, a first-order in time flux conserving algorithm [3], and resolved the instability.

3.1.4 2D Pressure-Driven

In Fig. 3.6 we plotted the average ABM simulations over two runs, and we can observe that, as in the 1D simulations (Fig. 3.5), the infection does not spread, and at initial times, in infection dominates the center of the ring structure, however, as time passes, the uninfected cells fall back into the center and the infected have peaks of concentration on the perimeter of that area. Representing again a complete failure of the treatment.

Results

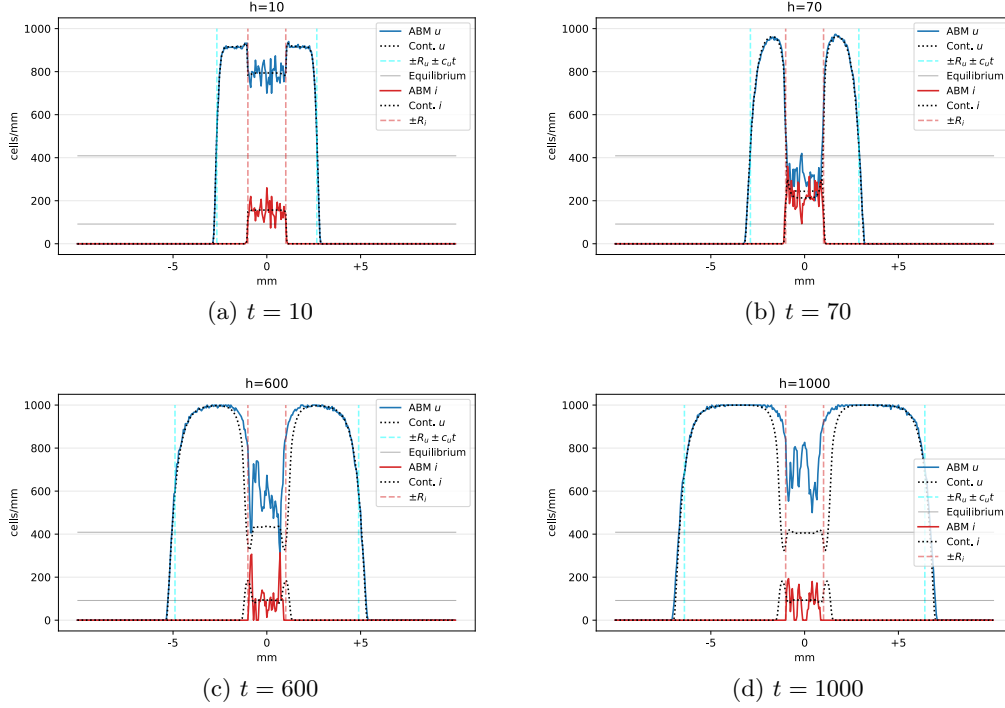


Figure 3.5: Results of 1D pressure-driven movement simulations of ABM average and continuum model

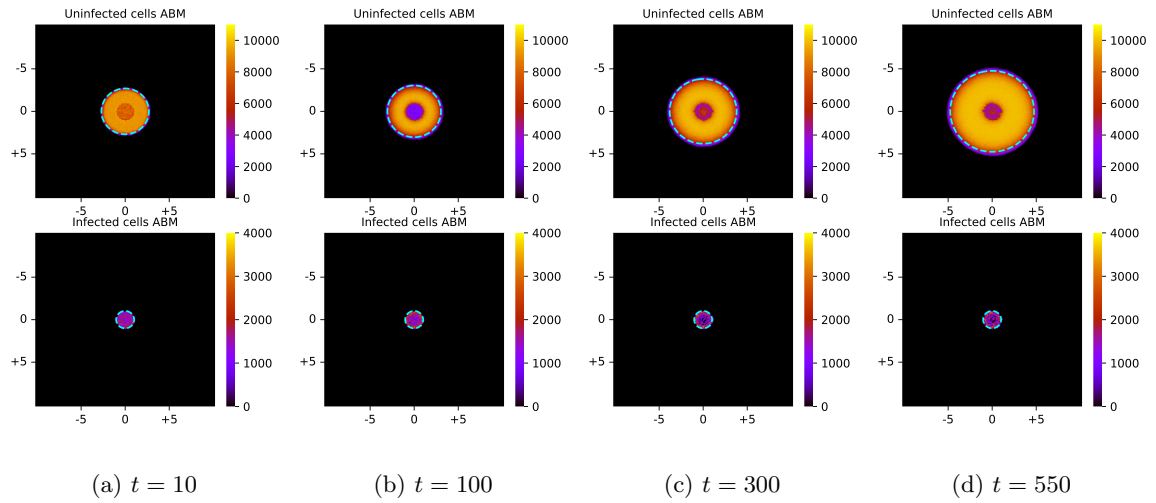


Figure 3.6: Results of 2D pressure movement simulations of ABM average

3.1.5 Other parameters

As Morselli in his original paper [9], we also consider the application of the therapy with different initial conditions, specifically a uniform distribution of the virus on the whole tumor, i.e. $R_i = R_u$, with the difference that we share the results of a single ABM simulation, instead of averaging. In Fig. 3.7 we plotted the ABM results of a single simulation with $\text{pop_unit} = 4$ for u because of the larger amount of cells, over the hours 70, 200, 400, 700, we observe the formation of the *disperse* infection structure presented in Wodarz et al. (2012) [12], as in Fig. 1.1.

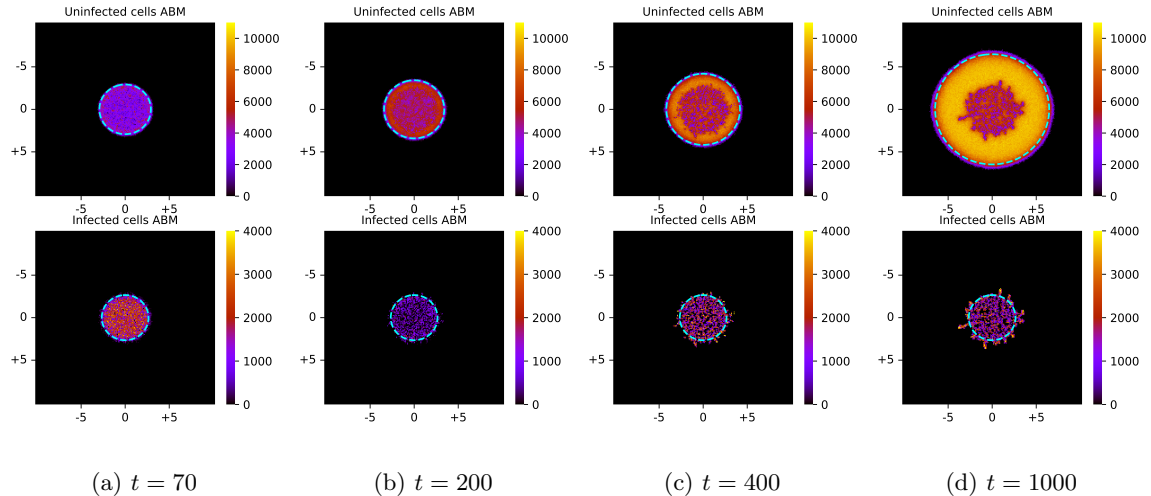


Figure 3.7: Results of 2D pressure movement simulations of ABM, such that $R_i = R_u$, above uninfected population with cyan dashed circle representing the expected wavefront from analytical results, below infected population with cyan dashed circle representing the initial radius R_i .

Suppose we deem that having more infected cells is a better outcome of the virotherapy. In that case, we may consider decreasing the value of the death rate parameter of infected cells q , which reduces u^* and increases i^* as discussed in the qualitative analysis (Fig. 2.3), if combined with the change of β to maximize i^* , with $\bar{\beta} = q + \sqrt{q^2 + pq}$, we will obtain larger i that might be helpful to spread the infection and for the number of antigens released to the immunological system. We selected $\tilde{q} = q/5 = 8.34 \times 10^{-3}$ and optimal $\bar{\beta}(\tilde{q}) = 2.33 \cdot 10^{-2}$, the new equilibrium is $(u^*, i^*) = (3570, 2858)$ in 2D, and the results for hours 70, 400, 700, 1000 are displayed in Fig. 3.8.

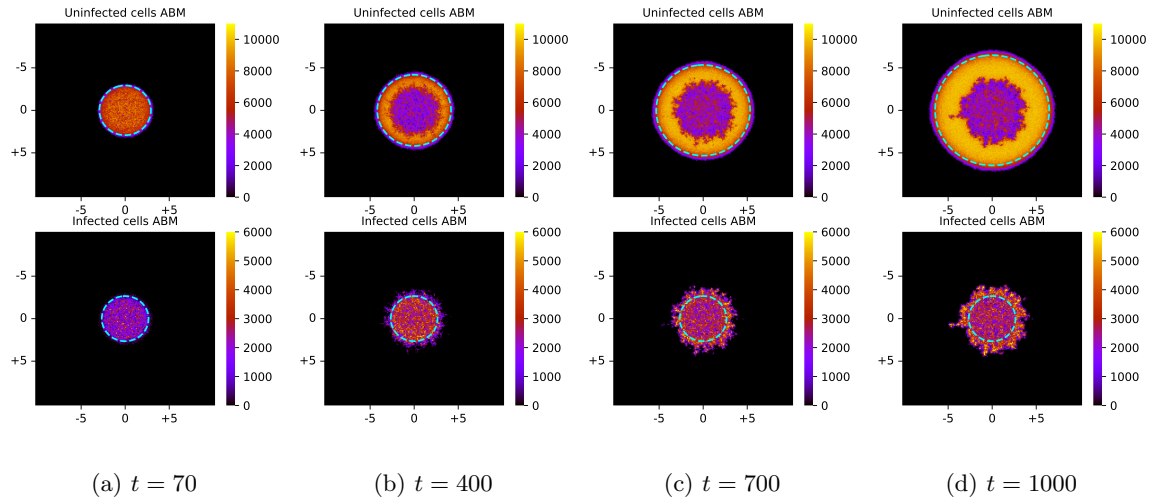


Figure 3.8: Results of 2D pressure movement simulations of ABM, such that $R_i = R_u$ and optimized q and β for the production of more infected cells, above uninfected population with cyan dashed circle representing the expected wavefront from analytical results, below infected population with cyan dashed circle representing the initial radius R_i .

3.2 Conclusion

We have successfully reproduced the results obtained by Morselli et al. (2023) [9], additionally, we have performed the qualitative analysis of their proposed continuum model to obtain further insights on how the parameters change the therapeutic outcome, both in terms of convergence of both uninfected and infected populations and in terms of their speed of propagation, except for the velocity of infected cells with the pressure-driven movement, for analytical results are still not available in literature.

Overall the simulations suggest that the tumor could not be treated with OVs alone considering the biologically-derived parameters, because the infection cannot completely extinguish the tumor cells. Interaction with the immunological system is an important addition to the model to obtain more realistic results, which is currently being developed by the same author, Morselli. Furthermore, the inclusion of chemotaxis and resource consumption is interesting to likely obtain also the *hollow ring* (Fig. 1.1), which we missed in our results with the reference parameters, in the original paper, decreasing the parameter q to one-tenth of the reference produced such structure.

Random undirected movement simulation demonstrated that OVs reduce the population of tumor cells both in the infected zone and in the wavefront of invasion (Fig. 3.2), while with the pressure-driven movement with reference parameters, it fails to spread the infection (Fig. 3.6). Starting the treatment with a uniformly distributed infected population over the domain of the tumor results in a better infection pattern for managing to continue with clustered infection in time, however, stochasticity plays an important role, especially in dimensions above 1D, because the infection has a low probability of spreading against the pressure and having more contact surface increases its chances of locally succeeding in branches or clusters.

Finally, we have changed the parameters correlated to the virus dynamics, q and β (Fig. 3.8), given our qualitative study, to increase the population of infected tumor cells expecting that in the future, engineered OVs with such parameters could be created, and the immune response to the increased production of TAA, TAN, and DAMPs would boost the success rate of the treatment.

Bibliography

- [1] Donald G. Aronson. Density-dependent interaction-diffusion systems. In WARREN E. STEWART, W. HARMON RAY, and CHARLES C. CONLEY, editors, *Dynamics and Modelling of Reactive Systems*, pages 161–176. Academic Press, 1980.
- [2] David R Berg, Chetan P Offord, Iris Kemler, Matthew K Ennis, Lawrence Chang, George Paulik, Zeljko Bajzer, Claudia Neuhauser, and David Dingli. In vitro and in silico multidimensional modeling of oncolytic tumor virotherapy dynamics. *PLoS Comput Biol*, 15(3):e1006773, March 2019.
- [3] Richard Courant, Eugene Isaacson, and Mina Rees. On the solution of nonlinear hyperbolic differential equations by finite differences. *Communications on Pure and Applied Mathematics*, 5(3):243–255, 1952.
- [4] Steven R. Dunbar. Traveling wave solutions of diffusive lotka-volterra equations: a heteroclinic connection in r4. *Trans. Amer. Math. Soc.*, (286):557–594, 1984.
- [5] Ela Guo and Hana M. Dobrovolny. Mathematical modeling of oncolytic virus therapy reveals role of the immune response. *Viruses*, 15(9), 2023.
- [6] Ke-Tao Jin, Wen-Lin Du, Yu-Yao Liu, Huan-Rong Lan, Jing-Xing Si, and Xiao-Zhou Mou. Oncolytic virotherapy in solid tumors: The challenges and achievements. *Cancers*, 13(4), 2021.
- [7] Amina Eladdadi Joseph Malinzi and Precious Sibanda. Modelling the spatiotemporal dynamics of chemovirotherapy cancer treatment. *Journal of Biological Dynamics*, 11(1):244–274, 2017. PMID: 28537127.
- [8] Dongwook Kim, Dong-Hoon Shin, and Chang K. Sung. The optimal balance between oncolytic viruses and natural killer cells: A mathematical approach. *Mathematics*, 10(18), 2022.
- [9] David Morselli, Marcello Edoardo Delitala, and Federico Frascoli. Agent-based and continuum models for spatial dynamics of infection by oncolytic viruses. *Bulletin of Mathematical Biology*, 85(10):92, Aug 2023.
- [10] Pannea Pooladvand, Chae-Ok Yun, A.-Rum Yoon, Peter S. Kim, and Federico Frascoli. The role of viral infectivity in oncolytic virotherapy outcomes: A mathematical study. *Mathematical Biosciences*, 334:108520, 2021.
- [11] W. Saarloos. Front propagation into unstable states. *Phys Rep*, 386, 08 2003.
- [12] Dominik Wodarz, Andrew Hofacre, John W. Lau, Zhiying Sun, Hung Fan, and Natalia L. Komarova. Complex spatial dynamics of oncolytic viruses in vitro: Mathematical and experimental approaches. *PLOS Computational Biology*, 8(6):1–15, 06 2012.

Bibliography

- [13] David Zwicker. py-pde: A python package for solving partial differential equations. *Journal of Open Source Software*, 5(48):2158, 2020.